Electronic Effects in Metal Complexation of C_{60}, $C_{59}N$, and $C_{59}B$

Feng Chen, David Singh, and Susan A. Jansen*

Department of Chemistry, Temple University, Philadelphia, Pennsylvania 19122

*Received: June 2, 1993; In Final Form: July 29, 1993**

The problem of rational design for doped fullerenes by chemical modification of C_{60}, though in its infancy, has been shown to be a fertile area of exploration. It is likely that modification of C_{60} will substantially enhance its electrical properties. Smalley et al. have synthesized boron-doped fullerene analogs. Other authors have shown that both endo- and exohedral substitution can readily occur for C_{60}. Synthetic initiatives in organometallic chemistry suggest that many late transition metal–ligand complexes can coordinate to the olefinic like C–C bond, primarily those involving platinum. In this report, we present a strategy for the design and evaluation of multiple substituted fullerenes and their complexes by a molecular orbital method based on extended Hückel theory. The focus is on the coordination site and bonding effects. Stability effects, redox behavior, and effect on cage reactivity are addressed, also.

Introduction

The discovery of superconductivity of M_xC_{60} (where M is an alkali metal, x = 1, 2, 3) has initiated a great interest in complexation and substitution of fullerenes. In particular, higher transition temperatures, T_c, within the range of 18 K in K_3C_{60} to 28 K in Rb_3C_{60} and 33 K in Cs_2RbC_{60} have been reported.[4] Superconductivity at 8.4 K in calcium-doped C_{60} has also been reported.[5] Furthermore, combinations of C_{60} with some alkali-metal alloys[6] ($KTl_{1.5}$, $RbTl_x$, CsTl, CsBi, and $CsHg_{1.1}$) have shown superconductivity. Recently, multiple synthetic objectives have been achieved including "chelation" with transition metals, doping C_{60} with boron and nitrogen to create donor and acceptor states, and chemical modification of C_{60}.[1,3] The preparation of boron-doped C_{60} analogs has been achieved.[1] The preparation of nitrogen-doped C_{60} has been reported and questioned.[7] Multiple theoretical analyses have addressed questions concerning the energy gap and solid state structure for alkali-metal complexes.[8] In this work, we have established a clearer understanding as to how the fullerene framework itself can be exploited further to produce complexes with enhanced electronic properties. In meeting these objectives, we have considered molecular level interactions which affect the formation of transition-metal C_{60} complexes. Applications of semiempirical methods have provided parameters for comparison and evaluation of substituted C_{60} analogs and have established general trends in reactivity. Here, we contrast the binding energy, HOMO–LUMO splitting of doped C_{60} and compare periodic trends in transition-metal chemistry. Moreover, the electronic properties of substituted analogs are discussed.

Computational Method

The analysis performed in this work was based on the extended Hückel methodology.[9] Though at the semiempirical level, the extended Hückel (EH) method has already shown great utility in the analysis of carbon-based systems[10] and graphitic materials.[11] As it was initially parametrized for hydrocarbon systems, EH has been used very successfully in multiple analyses of C_{60}.[12] In addition, the incorporation of transition metals into the EH protocol has provided the means to perform systematic studies of transition-metal complexes.[12] Such work on transition-metal systems has shown that the chemical trends produced are valid. The parameters used for this work are reported in Table I.

As the extended Hückel method cannot provide the minimized geometry, we have carefully constructed our model systems. In this work, two model geometries for C_{60} were used. The first was obtained from the minimized geometry reported by Hawkins et al.[13] In this geometry, localized bonding is observed though the difference in bond lengths is only about 0.02 Å. The second model is one in which all bond lengths are equal; the average C–C distance is the same for each model. These are referred to as localized and delocalized geometries, respectively. The final consideration in the model is the M–C_{60} complex geometry. Since there is limited structural data for these complexes, the metal–carbon distances were selected from organometallic models. Furthermore, to assure that trends produced would be relevant, the metal–carbon distance was varied to assess the effect of M–C distance on the trends established. No significant changes were produced in the energy or bonding trends upon variation of this distance.

TABLE I

atom	orbital	H_{ii}	ζ_1	ζ_2	c_1	c_2
C	2s	−21.40	1.62			
	2p	−11.40	1.63			
Sc	4s	−8.87	1.30			
	4p	−2.75	1.30			
	3d	−8.51	4.35	1.70	0.42	0.42
V	4s	−8.81	1.30			
	4p	−5.52	1.30			
	3d	−11.00	4.75	1.70	0.48	0.70
Mn	4s	−9.75	0.97			
	4p	−5.89	0.97			
	3d	−11.67	5.15	1.70	0.51	0.69
Fe	4s	−9.10	1.90			
	4p	−5.32	1.90			
	3d	−12.60	5.35	2.00	0.55	0.63
Ni	4s	−9.27	1.83			
	4p	−5.15	1.13			
	3d	−13.49	5.75	2.00	0.57	0.63
Cu	4s	−11.40	2.20			
	4p	−6.06	2.20			
	3d	−14.00	5.95	2.30	0.59	0.57
Ta	6s	−10.10	2.28			
	6p	−6.86	2.24			
	5d	−12.10	4.76	1.94	0.68	0.68

Results and Discussion

Analysis of C_{60}, $C_{59}B$, and $C_{59}N$. Our initial objective was to analyze the stability of substituted C_{60} moieties. We have evaluated the stability and analyzed the frontier orbital character modified by B and N substituents. Experimentally $C_{59}B$ is known and $C_{59}B$–NH_3 a Lewis acid/base adduct is also stable.[1,14] $C_{59}N$

* Abstract published in *Advance ACS Abstracts*, September 15, 1993.

0022-3654/93/2097-10958$04.00/0

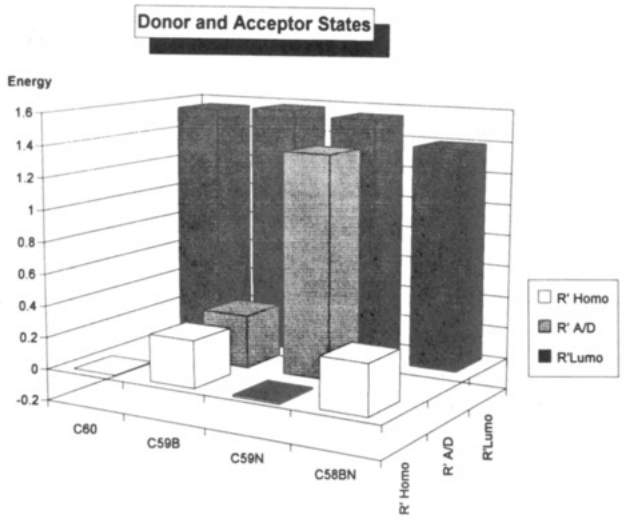

Figure 1. Frontier orbital diagram of C_{60}, $C_{59}B$, and $C_{59}N$. For boron the state shown is the acceptor state and for nitrogen this state is the donor state. The reference at 0 eV is the HOMO energy for C_{60}.

TABLE II: Assembly Energies (electronvolts) for Two Models of C_{60}, $C_{59}B$, and $C_{59}N$

	model geometry	CA energy	stabilization relative to C_{60}
C_{60}	localized	−304.50	0.00
	delocalized	−277.99	0.00
$C_{59}B$	localized	−302.80	1.70
	delocalized	−274.99	3.00
$C_{59}N$	localized	−293.60	10.90
	delocalized	−276.71	1.28

has not been successfully isolated though $C_{59}N_2$ and other nitrogen-substituted analogs have been reported.[7]

In the computation of the cluster assembly energy, two geometries were utilized—the localized and delocalized structures as described previously. The cluster assembly energies are shown in Table II. This energy represents the total bond energy in the cluster.

This analysis has established the importance of the model selection. The minimized structure is more representative of the "ground" electronic state in which some structural localization is expected. Though this geometry may not be as representative of the average molecular/electronic properties it should contribute to a greater degree to the reaction coordinate in the formation of C_{60} and related analogs and thus establish the trend observed in the cluster assembly energy when compared with experimental data. Therefore, it is not surprising that the experimental observations parallel the results obtained from the localized model. The greater instability in the localized model observed for $C_{59}N$ is attributed to population of antibonding π states of the buckyball framework which are destabilized to a greater extent in the localized structure.

The donor and acceptor properties of C_{60} have been established electrochemically and via salt/complex formation. Though high electron affinity, 2.65 eV, has been reported[15] for C_{60}, in reality it is not a "great" acceptor. Electrochemistry studies also show that oxidation, though difficult, can be achieved.[16] Substitution of carbon with boron or nitrogen is expected to modulate the redox characteristics thus enhancing the electronic properties and expanding the synthetic chemistry of C_{60}. The donor and acceptor states in $C_{59}B$ and $C_{59}N$ are shown in Figure 1. By comparison with typical semiconductors, boron or nitrogen acts as a donor/acceptor since each atom introduces a carrier state which can give rise to electrical conductivity. The donor/acceptor state convention used in this work follows from that of typical p-type and n-type semiconductors. (Typically group 3 dopants provide "defect" acceptor states and group 5 dopants give donor states.) From Figure 1, it can be ascertained that though $C_{59}B$ is "deficient" by an additional electron relative to C_{60}, only minor perturbation of the electronic structure occurs with substitution. The small difference in stabilization energy is due to depopulation of the orbitals that are mostly "nonbonding" C_{60} levels which comprise the set of HOMO orbitals, primarily. The stabilization energy differs for the two models as the average distance between cluster atoms is not the same for the two models. For nitrogen substitution, the acceptor level, which is singly occupied falls just below the LUMO. This is an antibonding π state and thus for the localized model provides for destabilization of the complex. This effect is offset but not completely compensated for by the slightly lower energies of the bonding orbitals containing nitrogen which fall below the HOMO. The magnitude of these effects vary with the model selected. These orbital characteristics may explain why nitrogen cannot be singly substituted into fullerenes as of yet. From these observations, it is reasonable to expect that the $C_{59}N$ cation will be stable if appropriate synthetic protocols can be achieved. In fact, our calculations show a more favorable cluster assembly energy for the $C_{59}N$ cation.

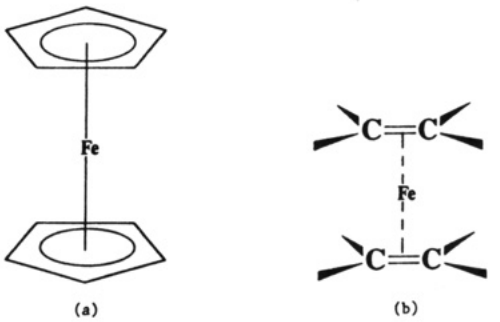

Figure 2. Coordination geometries for Fe–organometallic complexes.

Analysis of Transition-Metal Complexes of C_{60}, $C_{59}B$, and $C_{59}N$. Many transition-metal-substituted C_{60}'s have been prepared. Reports of La, Sc, Fe, and Ni with C_{60} complexes have been made.[2,17] In many cases, the metal coordinates exohedrally, e.g., to the exterior surface of the "ball". In some cases, the metal ion coordinates endohedrally. Our work has investigated the factors driving both endo- and exohedral coordination through molecular orbital interactions.

(*i*) *Fe–C_{60} Analogs.* Multiple reports have suggested that Fe–C_{60} analogs are stable. The report of the preparation of an Fe–C_{60} has recently appeared.[18] For our analysis we have focused on four primary sites. These sites are representative of Fe in its typical coordination, η^5 as in ferrocene and piano stool complexes, both interior and exterior sites and η^2 as in alkene complexes. These sites are shown in Figure 2.

The total binding energies, cluster assembly energies, and overlap populations for the local sites serve as parameters for the evaluation of site preference. The binding energy is computed by considering the Fe–C_{60} complex as the combination of two discrete fragments, Fe and C_{60}, and parallels the cluster assembly energy. The value of the binding energy represents the difference in the energy of the complex and the energy of the two discrete fragments. A comparison of the energies for these different models suggests that while binding of Fe may be favorable for all sites a stronger preference is observed for the η^2 sites. Further analysis of the overlap population, which is a measure of bond strength, for these two sites shows a preference for the 6,6′ C–C bond over the 5,6′ C–C bond. (The 5,6′ site describes a bond that links a five- and six-membered ring, the 6,6′ describes the link between two six-membered ring as shown in Figure 4.) The overlap population for a single Fe–C interaction 6,6′ is about 30% higher than it is for the 5,6′ site, and though perhaps trivial to note, there are two such interactions for each η^2 linkage. Another interesting characteristic of the bonding is that for the 6,6′ C–C, there is a

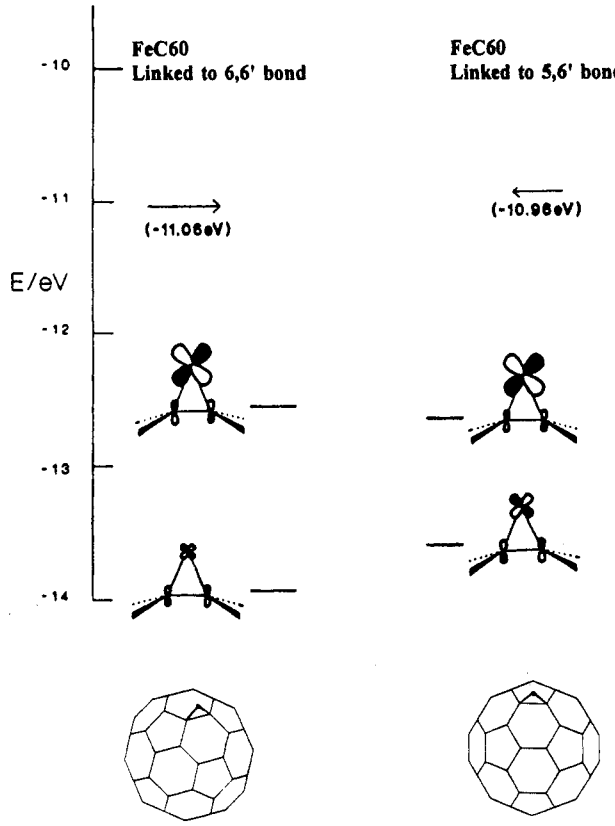

Figure 3. Orbital energy diagrams for 5,6′ and 6,6′ bonding site.

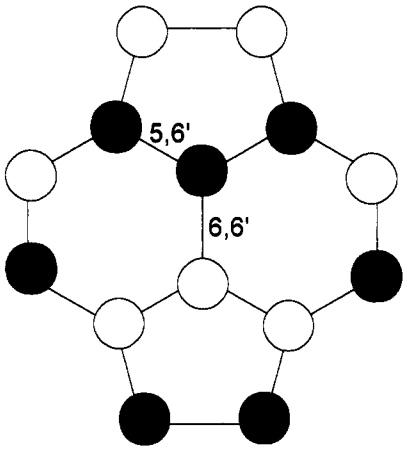

6,6' - Bond which is shared by two six-member rings
5,6' - Bond which is shared by five and six -member ring

Figure 4. LUMO of C_{60}.

severe reduction of C–C bond strength with metal chelation, suggesting significant olefinic character of the bond. No such reduction is observed for the 5,6′ C–C bond. The bonding interactions are shown in Figure 3.

In addition to these effects, significant changes occur that may effect the electronic properties of the Fe-chelated C_{60}. Turning to the analysis of the gross electronic changes produced by Fe bonding, shown in Figure 3, one notes a marked change in the HOMO–LUMO splitting for the two η^2 sites. The HOMO–LUMO splittings for the 6,6′ and 5,6′ sites are 1.06 and 0.65 eV, respectively. Generally speaking, the larger this splitting, the more stable the compound, as the effect that drives this gap is stabilization of bonding orbitals. Though the total energy of the two η^2 complexes are nearly equivalent, binding at the η^2-6,6′ site appears to be more favorable. The binding energy really represents the total energy of bonding in the complex. Since binding at the 6,6′ η^2 site effects reduction of C–C bond strength, the net binding energy is reduced by destabilization at the "olefinic" linkage. In the case of the 5,6′ site, no reduction of framework bonding occurs when the iron/C_{60} coordination occurs. Though the two binding energies are similar in magnitude, the complete picture of coordination/stability requires analysis of individual interactions. The unique bonding interactions responsible for Fe chelation are depicted in Figure 3. In Figure 3, it is apparent that the primary bonding orbitals are stabilized to differing degrees. In the 6,6′ case, the lowest bonding level is stabilized by about 0.3 eV relative to that level for 5,6′ binding, while the second orbital term is only slightly destabilized in the 6,6′ relative to the corresponding state for 5,6′ coordination. The degree of interaction of the metal with the framework orbitals of C_{60} is critically dependent on the relative energy of the metal and C_{60} states. For Fe, the d states fall just below the HOMO of C_{60}. Our calculations show that at limits beyond normal metal–C bonding, charge transfer occurs from the C_{60} to Fe effectively, filling the d states. Correspondingly, when Fe is placed endohedrally in the center of C_{60}, the population of the d states is 9.97 electrons, when the Fe approaches the "interior" wall of the C_{60}, the charge transfer is modulated by orbital interactions. When the two approach within normal η^2 bonding constraints, two effects are observed, coordinate bonding between Fe and the occupied C_{60} states and backbonding between Fe and C_{60}. The primary difference between the 5,6′ and the 6,6′ site in terms of their reactivity is the relative strength of backbonding. For the 6,6′ site, the increased backbonding provides greater population of C–C antibonding states and balances the $C_{60}\rightarrow$M donation. Thus the overlap population for the C–C at the 6,6′ η^2 site falls, but the overall charge transfer is not significant. For the 5,6′ η^2 site, the backbonding is not as efficient as the orbital localization differs for the two sites. For the 6,6′ site, the LUMO shows greater orbital density between the carbon atoms; however, for the 5,6′ site the orbital density is significantly lower. This is a consequence of the molecular symmetry constraints of C_{60}. Thus the backbonding interaction is greater for the 6,6′ site as greater orbital overlap can occur between the metal and the C_{60}. This explains the differences in the stabilization energy of the orbitals seen in Figure 3.

One final consideration in the analysis is the direction of charge transfer. Presently, a great deal of work on fullerenes has shown that the C_{60} moiety is electron deficient and that C_{60} anions form readily. Previous work has shown that a "self-doping" effect may occur upon chelation which actually results in loss of electron density to the chelating agent. For the η^2 sites considered here, the net effect is that the C_{60} moiety is oxidized relative to the native material. The greatest loss appears to occur in the case of the η^2 5,6′ site, in which a total of two electrons is lost from the C_{60}. For the η^2 6,6′ site, the oxidation is less severe with the loss of electrons occurring at the reactive site, primarily. This observation is consistent with the description of bonding trends presented previously.

In addition to consideration of Fe–C_{60} binding, we have focused on the interaction of many transition metals with C_{60}. Our analysis of the role of backbonding provides interesting insight in the trends produced. For these systems we have focused on the endo- and exohedral coordination of a variety of transition metals to an η^5 site and restricted the η^2 sites to the 6,6′ site. The selection of the particular transition metals was based on-going experimental work. Scandium–C_{60} complexes are well-known.[19] Cu–C_{60} complexes are not expected to be stable.[20] Tantalum and niobium carbides and Ta-doped graphites have high conductivities.[21] In the following discussion we will describe the trends established by considering the interactions of several transition metals with fullerenes.

(ii) Ta–C_{60} Analogs. Ta–C_{60}. Tantalum was selected for this analysis as TaC is a known superconductor and because tantalum has been used to produce more conductive graphitic materials.

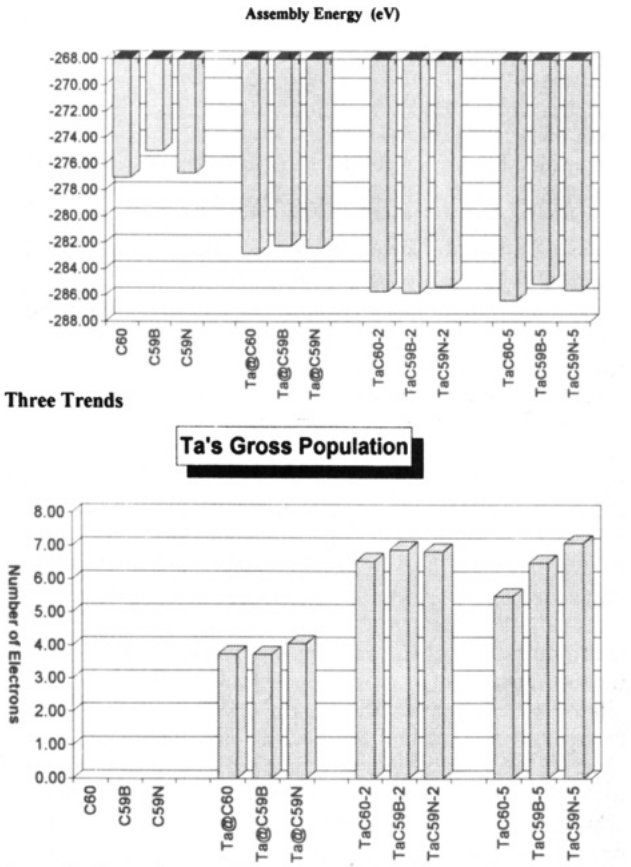

Figure 5. (a, top) Assembly energy of Ta@C_{60}, TaC_{60}, Ta@C_{59}B, TaC_{59}B, Ta@C_{59}N, and TaC_{59}N, where @ indicates η^5-endohedral substitution, 2 indicates coordination at 6,6′ site, and 5 represents η^5 exohedral coordinations. (b, bottom) Electronic population of Ta in Ta@C_{60}, TaC_{60}, Ta@C_{59}B, TaC_{59}B, Ta@C_{59}N, and TaC_{59}N.

It is expected that Ta–C_{60} complexes might be easily generated from tantalum doped graphites.

In this study, Ta is located in three different positions: (1) η^5 internal: Ta is trapped inside the C_{60} cage and sits in the center of a five-membered ring at equal distances to five carbon atoms; (2) η^5 external: Ta is located outside the C_{60} and above the center of five-membered ring. (3) η^2 external: Ta is outside the C_{60} and located above the bond which links two six-membered rings the so-called η^2 6,6′ site.

In Figure 5 the relative complex stability for each complex is shown. It can be seen that Ta prefers "external" η^5 or η^2 coordination. From the results shown here and the analysis, it is clear that bonding limits inside the ring are weaker and that the direction of charge transfer is affected by coordination. The charge transfer is a direct result of covalent effects which are at a minimum in endohedral coordination. For endohedral η^5 complexes of tantalum, the metal is oxidized while it is reduced somewhat when coordinated at the exohedral site. This is observed because the orbital localization favors exohedral coordination as both the $C_{60}\rightarrow$M and M$\rightarrow C_{60}$ mechanisms are more active. In fact, the M$\rightarrow C_{60}$ mechanism is probably more active in tantalum complexes relative to Fe–C_{60} as the metal d states are closer in energy to the frontier states of C_{60}. The overlap population is much greater for Ta–C bonding in the exohedral site, 0.4016 relative to that of endohedral Ta–C bond, 0.15. It is interesting to note, also, that backbonding more strongly favors the exohedral coordination. The C–C bond strength, an indicator of backbonding is reduced by about 20% relative to free C_{60} for the exohedral coordination, while it is reduced only 7–8% for the endohedral coordination. Since the d states of Ta are close in energy to reactive orbital states of C_{60}, the interaction serves to create new bonding and antibonding Ta–C states. Since initially all of the d states of tantalum are centered at an energy below

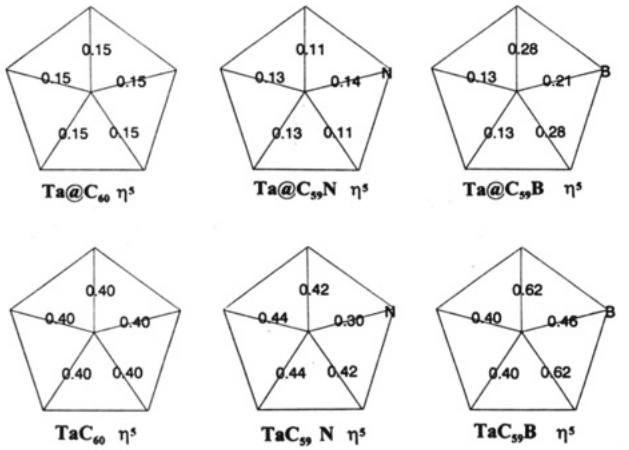

Figure 6. Overlap population for Ta-X bonds in Ta@C_{60}, TaC_{60}, Ta@C_{59}B, TaC_{59}B, Ta@C_{59}N, and TaC_{59}N.

the HOMO of C_{60}, after reaction, a significant percentage of the d states are destabilized to a level above the HOMO and thus the corresponding electrons are redistributed into nonbonding C_{60} states near the frontier. This charge-transfer effect can be compensated for by other orbital interactions as described previously; however, these effects are much weaker for the endohedrally coordinated Ta.

The η^2 coordination mechanism appears similar to that of Fe. Strong Ta–C bonding is observed with a corresponding reduction in the C–C bonding at the site where coordination occurs. The corresponding overlap populations are 0.57 for Ta–C and 0.86 for the associated C–C.

The assembly energies and binding energies of Ta complexes show that endo- and η^5 exohedral bonding is favorable for the C_{60}.

Boron- and Nitrogen-Substituted Ta–C_{60} Analogs. Keeping the same conditions, substitution of one carbon atom in the five-membered ring by B or N has been considered also. Substitution of boron provides little deformation of the C_{60} icosohedron; substitution of N causes greater distortion. For complexation at the η^2 site, the carbon substituted is one which is involved in binding to the metal substituent. The observation for the endohedral η^5 sites shows more interesting features. When Ta is bound to the five-membered ring, exohedrally, there are significant differences in the tantalum–ring binding. More interesting is the observation that the Ta–C overlap population as shown in Figure 6, for the carbon atoms adjacent to the boron is about 50% larger in the case of boron substitution as it is in the pristine C_{60}, a corresponding reduction in the ring binding is observed also. This is due to the localization effects induced by the difference in the electronegativities of carbon and boron. Such an observation suggests an increased instability in the fullerene unit that may be exacerbated by further reduction of the complex. No such effort is observed for C_{59}N, in fact, metal–ring binding is very similar to that of C_{60}. The assembly energies of these complexes and corresponding charges of Ta and C_{59}X derivatives are shown in Figure 5. The trends are similar for the boron- and nitrogen-substituted fullerenes. As in the case of C_{60}, the endohedral substitution provides an "oxidized" tantalum and the exohedral substitution effects a net "reduction" of the tantalum metal.

The effect of tantalum substitution on the frontier orbital levels, i.e., the donor/acceptor states for the Ta@C_{60}-nX_n, where X = B or N, complex is shown in Figure 7. In all cases of tantalum substitution, the HOMO–LUMO gap decreases and "defect" states, nonbonding states of tantalum become active for several tantalum fullerene derivatives. This observation suggests that tantalum substitution, if achieved synthetically, should result in materials of enhanced conductivities.

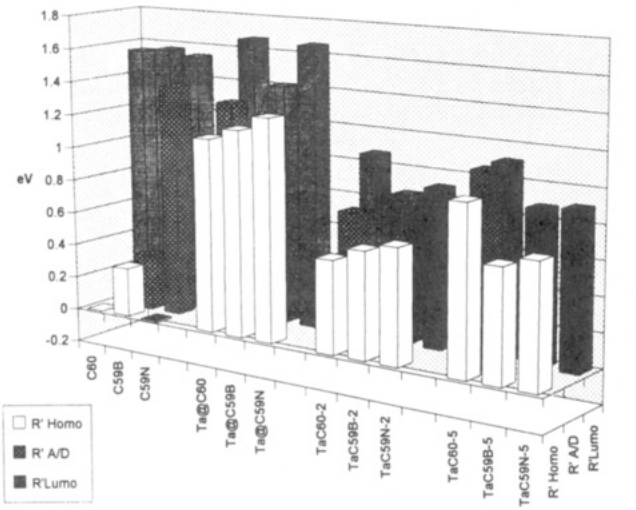

Figure 7. Frontier orbital diagram of $Ta@C_{60}$, TaC_{60}, $Ta@C_{59}B$, $TaC_{59}B$, $Ta@C_{59}N$, and $TaC_{59}N$.

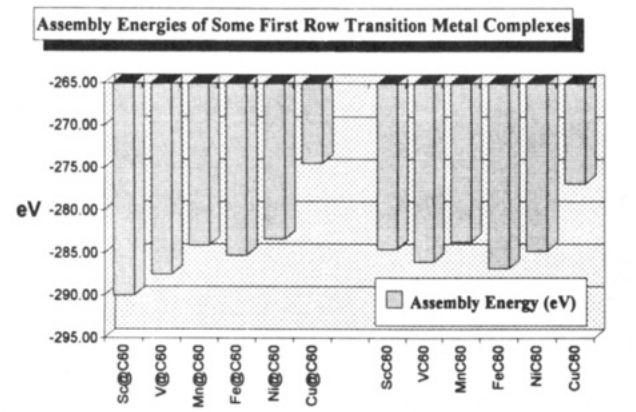

Figure 8. Assembly energies of first row transition metals (Sc, V, Mn, Fe, Ni, Cu) with C_{60}.

(*iii*) *Periodic Effects.* The final objective in this work was to establish trends in electronic properties of the C_{60} complexes with first-row transition metals. It is well-known that scandium can complex endohedrally, in fact, trimers of scandium are stable when incorporated into the C_{82} icosohedron.[19] To date, the successful complexation of copper has not been achieved. The endohedral incorporation of iron in C_{60} has been questioned as well. In this component of our work we summarize the major effects for a few transition metals in the first period, Sc, V, Mn, Fe, Ni, and Cu. These are chosen to survey the bonding effects for the transition metals. We first discuss effects for early transition metals. The analysis will then be extended to copper to understand why reactions with copper have failed to produce any substituted C_{60} complexes. In this work, each transition metal is bound at two positions, the η^5 (internal) and η^2 (external) of C_{60}. The analysis is limited to the two sites—the η^5 endohedral as this is the only anticipated internal site and the η^2 exohedral as this site appears to the most stable for all metals considered thus far. The assembly energy, frontier state energies, and population trends were calculated. The assembly energies/binding energies are favorable for all η^5 sites except that of copper. These data are provided in Figure 8. Though it is not possibly to establish a complete trend from the survey provided, two features are apparent in the analysis of the data. First, a periodic tendency in binding energy is observed as the binding/assembly energies fall across the first period. The observation that copper–C_{60} binding is energetically unfavorable supports the experimental evidence which suggests Cu–C_{60} is not as stable as other fullerene materials. Two effects drive these observation. The first is the atomic orbital energies of the transition metal and the second is the metal d-orbital population. In general, the orbital energies fall from scandium to copper, thus affecting the orbital composition of the new M–C_{60} states. This can be understood by an analysis of the extreme cases. For scandium the d states are at a level just higher than the LUMO states of C_{60}. This means that all of the bonding orbital combinations between C_{60} and Sc have a considerable higher carbon contribution, the corresponding antibonding contributions have greater scandium contributions in turn. For copper, the d (and s) states fall below the frontier states of C_{60} and thus metal complexation destabilizes the bonding C_{60} orbital by the process described previously.

In addition, the net population of states effects the total stability. In the case of scandium, the metal atom contributes three electrons to the resulting states, for copper the combination is 11 electrons. Thus, the new states formed by scandium are electron deficient and M–C_{60} bonding is weak. In fact reduction is expected to favor Sc–C_{60} binding. In the case of copper, the metal–carbon bonding and a significant percentage of antibonding states become filled while most of the corresponding states remain unoccupied in the early transition metal derivatives. In particular, the population of the Cu s state and the relatively low s-orbital energy implicate the s levels in bonding for Cu almost exclusively. In this analysis the s state of copper is at a low energy relative to the frontier states of C_{60} and thus multiple interactions between the C–C bonding orbitals are affected. Since the s energy is low relative to these states, the C_{60} states are destabilized and in particular, weakening of the C–C at the metal binding site is observed. As a result the interaction of Cu with C_{60} is destructive to the C_{60} framework as the buckyball is destabilized through the orbital interaction and population of antibonding states—a direct result of the lower orbital energies of Cu and the high population of Cu valence states. Thus the assembly energy is actually less for Cu–C_{60} than it is for C_{60} and the binding energy is repulsive. A similar case is observed for the η^2 bonding, that is the early transition metals show attractive binding potential with the binding of copper being energetically unfavorable. Similar trends are reflected in the orbital interactions. That is, the binding energy decreases toward copper. In addition, the metal–carbon interaction appears characteristic of the electronic properties of the metal. In the case of Sc–C the metal–carbon overlap population is at a minimum overall, though favorable M–C bonding occurs. This is likely due to weaker backbonding effects as the gross population of states is lower for the Sc system than the other metals. Less destabilization of the fullerene framework occurs with Sc complexation. As the metal d-state population increases, an increase in metal–carbon overlap population is observed with the corresponding decrease in C–C bond strength. This effect is observed upon varying the metal from scandium to vanadium to iron. The overall decrease in cluster energy is due to weakening of framework bonding through the charge redistribution effects initiated by metal–carbon bonding.

From the data shown in assembly energies and the HOMO/LUMO state diagram in Figure 9, it can be concluded that the early transition metals may form stable complexes with $C_{59}B$ and $C_{59}N$ as well as C_{60}. Again, the direction of charge transfer and bonding depends on the relative orbital energies of the transition metal and the subsequent population of the orbitals of the metal–fullerene complex as shown in Figure 9. One interesting effect is that in all cases, endohedral substitution results in greater donation from the metal to C_{60}, thus careful analysis of the oxidation state of the metal atoms in a series of standards may help in establishing coordination sites.

The η^2 and η^5 Sc–C_{60} binding sites do not appear as favorable as other metals. Formation of the endohedral scandium trimer in which Sc–Sc interactions can occur will provide a unique set of energy states that will demonstrate different limits of binding within the fullerene framework. A discussion of such metal cluster formation will be forthcoming.

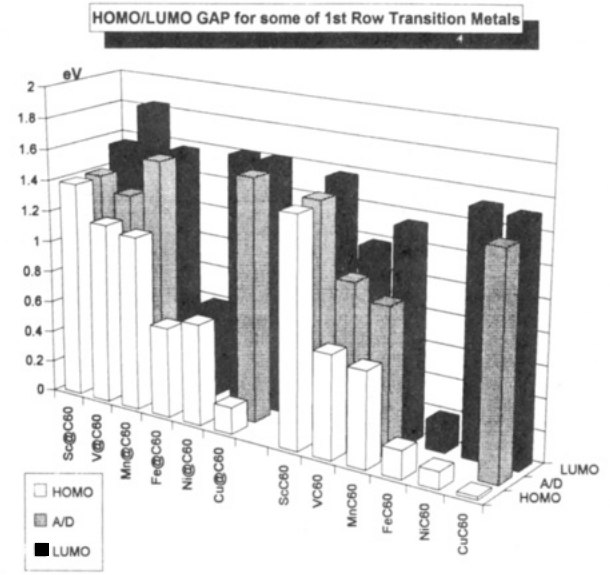

Figure 9. Frontier orbital diagram of first row transition metals (Sc, V, Mn, Fe, Ni, Cu) with C_{60} complexes.

Conclusions

The choice of complexing metals is important in establishing rational design protocols as the framework of the fullerene is fragile and charge redistribution can effect its stability. Donor and acceptor states from the nitrogen- and boron-substituted C_{60} derivatives offer a degree of variation in complexation and redox objectives, in particular, the boron-substituted analogs appear more chemically active than the nitrogen homologs, though their fullerene cage may suffer greater instability upon reaction. Transition-metal complexes show stability both for multiple coordination sites: η^5 external, η^5 internal, and η^2 sites each appearing stable for most earlier transition metals. Cu–C_{60} is not energetically favored for any site due to orbital energy effects and the relatively high population of antibonding levels. It seems that the fullerene cage will open upon complexation with copper. Finally, the direction of charge transfer and redox state of the metal may be a direct indicator of endohedral versus exohedral coordination. Careful experimental parameterization of metal charge may help establish the coordination geometry for M–C_{60} complexes.

Finally, this work, though directed at analysis of metal complexation of fullerenes, also provides some insight into adsorption properties of C_{60} on metal substrates. Typically the surface binding/adhesion is driven by local bonding effects which are adequately described by application of the EH method, and relevant bonding trends are established in this report.

Acknowledgment. We gratefully acknowledge financial support for this work from the AFOSR, Grant F49620-93-1-0018 and Professor Harry Rappaport for his useful disscussions.

References and Notes

(1) Guo, T.; Jin, C. M.; Smalley, R. E. *J. Phys. Chem.* **1991**, *13*, 4948–4950.

(2) (a) Heath, J. R.; O'Brien, S. C.; Zhang, Q.; Liu, Y.; Curl, R. F.; Kroto, H. W.; Smalley, R. E. *J. Am. Chem. Soc.* **1985**, *107*, 7779–7780. (b) Cioslowski, J.; Fleischmann, E. D. *J. Chem. Phys.* **1991**, *94*, 3730–3734. (c) Cioslowski, J. *J. Am. Chem. Soc.* **1991**, *113*, 4139–4141. (d) Weiske, T.; Bohme, D. K.; Hrusak, J.; Kraetschmer, W.; Schwarz, H. *Angew. Chem. Int. Ed. Engl.* **1991**, *30*, 884–886. (e) Caldwell, K. A.; Giblin, D. E.; Hsu, C. S.; Cox, D. M.; Gross, M. L. *J. Am. Chem. Soc.* **1991**, *113*, 8519–8521. (f) Chai, Y.; Guo, T.; Jin, C. M.; Haufler, R. E.; Chibante, L. P. F.; Fure, J.; Wang; Alford, J. M.; Smalley, R. E. *J. Phys. Chem.* **1991**, *95*, 7564–7568. (g) Cioslowski, J.; Nanayakkara, A. *J. Chem. Phys.* **1992**, *96*, 8354–8362.

(3) (a) Fagan, P. J.; Calabrese, J. C.; Malone, B. *Science* **1991**, *252*, 1160–1161. (b) Fagan, P. J.; Calabrese, J. C.; Malone, B. In *Fullerenes*; Hammod, G. S., Kuck, V. J., Eds.; ACS Symposium Series 481; American Chemical Society: Washington, DC, 1992; Chapter 12, pp 177–186. (c) Fagan, P. J.; Calabrese, J. C.; Malone, B. *J. Am. Chem. Soc.* **1991**, *113*, 8957–8958.

(4) (a) Hebard, A. F.; Rosseinsky, M. J.; Haddon, R. C.; Murphy, D. W.; Glarum, S. H.; Palstra, T. T. M.; Ramirez, A. P.; Kortan, A. R. *Nature*, **1991**, *350*, 600–601. (b) Rosseinsky, M. J.; Ramirez, A. P.; Glarum, S. H.; Murphy, D. W.; Haddon, R. C.; Hebard, A. F.; Palstra, T. T. M.; Kortan, A. R.; Zahurak, S. M.; Makhija, A. V. *Phys. Rev. Lett.* **1979**, *66*, 2830–2832. (c) Tanigaki, K.; Ebbesen, T. W.; Saito, S.; Mizuki, J.; Tsai, J. S.; Kubo, Y.; Kuroshima, S. *Nature* **1991**, *352*, 222–223.

(5) Kortan, A. R.; Kopylov, N.; Glarum, S. H.; Gyorgy, E. M.; Ramirez, A. P.; Fleming, R. M.; Thiel, F. A.; Haddon, R. C. *Nature* **1992**, *355*, 529–532.

(6) (a) Kraus, M.; Freytag, J.; Gartner, S.; Veith, H. M.; Kraetschmer, W.; Luders, K. *Z. Phys. B: Condens. Matter* **1991**, *85*, 1–2. (b) Kraus, M.; Gartner, S.; Baenitz, M.; Kanowski, M.; Vieth, H. M.; Simmons, C. T.; Kraetschmer, W.; Thommen, V.; Lang, H. P.; Guntherodt, H. J.; Luders, K. *Europhys. Lett.* **1991**, *17*, 5.

(7) Pradeep, T.; Vijayakrishnan, V.; Santra, A. K.; Rao, C. N. R. *J. Phys. Chem.* **1991**, *95*, 10564–10565.

(8) (a) Zhang, Z.; Chen, C. C.; Kelty, S. P.; Dai, H.; Lieber, C. M. *Nature* **1991**, *353*, 333–335. (b) Regueiro, M. N.; Monceau, P.; Rassat, A.; Bernier, P. P.; Zahab, A. *Nature* **1991**, *354*, 289–291. (c) Rotter, L. D.; Schlesinger, Z.; McCauley, J. P., Jr.; Coustel, N.; Fischer, J. E.; Smith, A. B., III *Nature* **1991**, *355*, 532–534. (d) Saito, Y.; Shinohara, H.; Kato, M.; Nagashima, H.; Ohkohchi, M.; Ando, Y. *Chem. Phys. Lett.* **1992**, *189*, 236–240. (e) Takahashi, T.; Suzuki, S.; Morikawa, T.; Katayama-Yoshida, H.; Hasegawa, S.; Inokuchi, H.; Seki, K.; Kikuchi, K.; Suzuki, S.; Ikemoto, K.; Achiba, Y. *Phys. Rev. Lett.* **1992**, *68*, 1232–1235.

(9) Hoffmann, R. *J. Chem. Phys.* **1963**, *39*, 1397.

(10) Hoffmann, R.; Lipsomb, W. M. *J. Chem. Phys.* **1962**, *36*, 3179.

(11) Hoffmann, R.; Lipsomb, W. M. *J. Chem. Phys.* **1962**, *37*, 2872.

(12) Haymet, A. D. J. *J. Am. Chem. Soc.* **1986**, *108*, 319–321.

(13) (a) Hawkins, J. M.; Lewis, T. A.; Loren, S. D.; Meyer, A.; Heath, J. R.; Shibato, Y.; Saykally, R. J.; *J. Org. Chem.* **1990**, *55*, 6250–6252. (b) Hawkins, J. M.; Meyer, A.; Lewis, T. A.; Loren, S. D.; Hollander, F. J. *Science* **1991**, *252*, 312–313.

(14) Andreoni, W.; Gygi, F.; Parrinello, M. *Chem. Phys. Lett.* **1992**, *190*, 159–162.

(15) Haddon, R. C. *Acc. Chem. Res.* **1992**, *25*, 127–133.

(16) (a) Kroll, G. H.; Benning, P. J.; Chen, Y.; Ohno, T. R.; Weaver, J. H.; Chibante, L. P. F.; Smalley, R. E. *Chem. Phys. Lett.* **1991**, *181*, 112–116. (b) Vassallo, A. M.; Pang, L. S. K.; Cole-Clarke, P. A.; Wilson, M. A. *J. Am. Chem. Soc.* **1991**, *113*, 7820–7821.

(17) (a) Huang, Y.; Freiser, B. S. *J. Am. Chem. Soc.* **1991**, *113*, 8186–8187. (b) Rosen, A.; Waestberg, B. *J. Am. Chem. Soc.* **1988**, *110*, 8701–8703.

(18) Roth, L. M.; Huang, Y.; Schwedler, J. T.; Cassady, C. J.; Ben-Amotz, D.; Kahr, B.; Freiser, B. S. *J. Am. Chem. Soc.* **1991**, *113*, 6298–6299.

(19) (a) Shinohara, H.; Saito, H.; Ohkohchi, M.; Ando, Y.; Kodama, T.; Shida, T.; Kato, T.; Saito, Y. *Nature* **1992**, *357*, 52–54. (b) Yannoni, C. S.; Hoinkis, M.; de Vries, M. S.; Bethune, D. S.; Salem, J. R.; Crowder, M. S.; Johnson, M. E. *Science* **1992**, *256*, 1191–1192.

(20) Wang, P.; Shamsuzzoha, M.; Wu, X. L.; Lee, W. J.; Metzger, R. M. *J. Phys. Chem.* **1991**, *96*, 9025–9028.

(21) Linker, G.; Greerk, J. *Solid State Commun. 48* (12), 1089–1092.